International Institute for
Applied Systems Analysis
IIASA www.iiasa.ac.at

Singular Homoclinic Bifurcations in Tri-trophic Food Chains

Feo, O. de & Rinaldi, S.

IIASA Working Paper

WP-96-076

July 1996

Working Paper

Singular homoclinic bifurcations in tri-trophic food chains

O. De Feo and S. Rinaldi

WP-96-76
July 1996

IIASA International Institute for Applied Systems Analysis □ A-2361 Laxenburg □ Austria
Telephone: +43 2236 807 □ Fax: +43 2236 71313 □ E-Mail: info@iiasa.ac.at

Singular homoclinic bifurcations in tri-trophic food chains

O. De Feo and S. Rinaldi

WP-96-76
July 1996

International Institute for Applied Systems Analysis □ A-2361 Laxenburg □ Austria
Telephone: +43 2236 807 □ Fax: +43 2236 71313 □ E-Mail: info@iiasa.ac.at

Singular homoclinic bifurcations in tri-trophic food chains

O.De Feo(°) *and S. Rinaldi*(°°)

(°) CIRITA, Politecnico di Milano, Via Ponzio 34/5, 20133 Milano, Italy.

(°°) Centro Teoria dei Sistemi, CNR, Politecnico di Milano, Via Ponzio 34/5, 20133 Milano, Italy.

Abstract

The Rosenzweig-MacArthur food chain model is proved to have homoclinic orbits. The proof is in two steps. First we use a geometric approach based on singular perturbation and detect singular homoclinic orbits as well as parameter combinations for which these orbits exist. Then we show, numerically, that for slightly different parameter values there exist also non singular homoclinic orbits which tend toward the singular ones when the time responses of the three trophic levels are extremely diversified. The analysis is performed systematically, without exploiting too deeply the mathematical structure of the Rosenzweig-MacArthur model. This is done intentionally, in order to facilitate readers interested more in the methodology than in the application to food chains.

1 Introduction

Tri-trophic food chains have been extensively studied during the last decades. The most recent investigations [1], [2], [3] deal with the standard Rosenzweig-MacArthur model and show that its bifurcation structure is quite rich. In particular, it comprises a complex cascade of intersecting flip and tangent bifurcations of cycles delimiting the region of chaotic behavior [3].

Although these analyses are restricted to local bifurcations, they clearly indicate the existence of global bifurcations. Indeed, *homoclinic orbits*, *i.e.*, orbits tending toward the same saddle forward and backward in time, have been numerically detected in [2], [3].

The proof of existence (or non existence) of homoclinic orbits is a strategic point for the analysis of any nonlinear dynamical system. In fact, homoclinic orbits exist only for particular parameter combinations and are substituted by very special behaviors, including cycles and strange attractors, when the parameters are perturbed generically. Finding *homoclinic bifurcations*, *i.e.*, parameter combinations that guarantee the existence of homoclinic orbits, is certainly a very difficult task, even if there have been recent progresses in the field [4].

Aim of this paper is to show how homoclinic orbits in the Rosenzweig-MacArthur model can be easily detected in the case of trophic levels with

time responses increasing from bottom to top. When this hierarchical order is taken to the limit of highly diversified dynamics, the analysis of the system can be performed through *singular perturbation* [5]. Such technique has already been used to study the cyclic behavior of tri-trophic food chains [6], [7] as well as other problems in population dynamics, like competitive coexistence [8] and insect outbreaks in forest-ecosystems [9], [10]. Singular perturbation has also been used to detect homoclinic orbits but only in the simplest case of second order systems [11].

The paper is organized as follows. In the next section some background information on slow-fast systems and singular orbits is given. In particular, singular saddles and singular homoclinic orbits are defined. In Sect. 3 the Rosenzweig-MacArthur model is presented and its singular orbits are determined. The analysis is divided into three steps in order to facilitate readers more interested in the methodology than in the application to food chains. The conclusion is that singular homoclinic orbits exist for suitable parameter values. Then, in Sect. 4 the analysis is completed by looking at the non singular case. Numerical experiments show that also in that case homoclinic orbits exist for slightly different parameter values and tend toward the singular ones when the time responses of prey, predator and superpredator are highly diversified.

2 Slow-fast systems and singular orbits

Dynamical systems are usually composed of interacting compartments and these compartments are very often characterized by highly differentiated time responses. Systems of this kind are called slow-fast systems and the case considered in this paper is that of third order systems of the form

$$\dot{x} = f(x, y, z) \tag{1a}$$

$$\dot{y} = \varepsilon g(x, y, z) \tag{1b}$$

$$\dot{z} = \varepsilon^2 h(x, y, z) \tag{1c}$$

where ε is a small and positive constant parameter. Thus, the state variables x, y and z are, respectively, the fast, intermediate, and slow component of the system. The analysis of slow-fast systems usually refers to the case of only two dynamically diversified compartments [5]. Eqs. (1), on the contrary, describe a system with a three level hierarchy in its dynamics. Systems of this kind have already been described in the literature (see, for example, [6], [7]).

Orbits of system (1) can be approximated by so-called singular orbits, which are easily obtained by concatenating orbits of three very simple first order systems, called, *fast*, *intermediate* and *slow*.

The fast system is

$$\dot{x} = f(x, y, z)$$

where y and z are frozen at constant values. Thus, the manifold $f = 0$ is the equilibrium manifold of the fast system embedded in the three-dimensional space (x, y, z) and singular orbits starting from a generic point (*i.e.*, a point which is not an equilibrium point of the fast system) have a first segment parallel to the x axis. Equilibria of the fast system can be linearly stable or unstable (depending upon the sign of f_x) so that the manifold $f = 0$ can be partitioned into stable and unstable manifolds, separated by lines which are bifurcations of the fast system with respect to y and z.

In the example shown in Fig.1, the fast system has multiple equilibria, and its bifurcations are fold bifurcations. The first piece of the singular orbit is the fast segment 0 1 connecting the initial point 0 to a stable equilibrium point of the fast system. Other fast segments can be present in a singular orbit. For example, segment 6 7 in Fig.1 is a fast segment initiating at a fold point of the fast system.

The intermediate system is defined on the manifold $f(x, y, z) = 0$ and is described by

$$\dot{y} = g(x, y, z)$$

where z is frozen at a constant value. This means that all intermediate segments of singular orbits are lines obtained by intersecting the manifold $f = 0$ with a plane parallel to the (x, y) plane. The singular orbit depicted

in Fig.1 contains four intermediate segments (namely 1 2, 3 4, 5 6, and 7 8). These segments terminate at an equilibrium of the intermediate system, *i.e.*, on the line $f = g = 0$, or at a bifurcation point of the fast system(*e.g.*, point 6 in Fig.1).

Finally, the slow system is defined on the manifold $f = g = 0$ and is described by

$$\dot{z} = h(x, y, z)$$

The slow segments are therefore pieces of the line $f = g = 0$ with the direction of the flow dictated by the sign of h (see segments 2 3 and 4 5 in Fig.1). They terminate either at an equilibrium point (characterized by $f = g = h = 0$), or at a bifurcation point of the intermediate system (like points 3 and 5 in Fig.1).

By properly connecting fast, intermediate and slow segments one can easily generate singular orbits, as shown in Fig.1. The procedure terminates when an equilibrium is reached or when a concatenation point coincides with one of the previously generated points, in which case a *singular cycle* is obtained. The main result of singular perturbation theory is that any orbit of system (1) approaches, for $\varepsilon \to 0$, the corresponding singular orbit. Of course, such a result holds provided the functions f, g, and h satisfy suitable conditions. For singular orbits not passing through critical points this result

has been proved by Tikhonov [12], while for singular orbits passing through folds the result is proved in [13] (see also [14] for a modern presentation of this topic).

A *singular saddle* is an equilibrium point with an incoming and an outcoming singular orbit. A degenerate, but interesting, singular orbit is the *singular homoclinic orbit.* It can be defined as a singular orbit that tends toward the same equilibrium point both forward and backward in time. Consistently, the equilibrium point is a singular saddle, which has an outcoming singular orbit that returns exactly to it. As in the standard case, singular homoclinic orbits can be obtained by varying a strategic parameter until a singular saddle collides with a singular cycle. In the next section this property is used to prove the existence of singular homoclinic orbits in the Rosenzweig-MacArthur model.

3 Slow-fast food chains

Rosenzweig-MacArthur model is the most popular model of tri-trophic food chains [1], [2], [3]. It assumes that the prey (x) has logistic growth and that predator (y) and superpredator (z) have Holling type II functional response. In the majority of food chains, the size of individuals and the time they need for reproduction and growth are increasing with the trophic level.

Phytoplankton-zooplankton-fish is a typical example, but almost all food chains belonging to the class plant-herbivore-carnivore have time responses increasing along the chain from bottom to top. Thus, after scaling the dynamics of the three trophic levels by means of a dimensionless positive parameter ε, the model takes the form [7]

$$\dot{x} = x\left[r\left(1-\frac{x}{K}\right)-\frac{a_1 y}{b_1+x}\right] = xF(x,y) \tag{2a}$$

$$\dot{y} = \varepsilon y\left[\frac{c_1 x}{b_1+x}-\frac{a_2 z}{b_2+y}-d_1\right] = \varepsilon y G(x,y,z) \tag{2b}$$

$$\dot{z} = \varepsilon^2 z\left[\frac{c_2 y}{b_2+y}-d_2\right] = \varepsilon^2 z H(y) \tag{2c}$$

where the ten parameters r, K, a_i, b_i, c_i, d_i, $i = 1,2$ are positive. Model (2) has two particular features: (i) it is a positive model because $f = xF$, $g = yG$, $h = zH$; (ii) F does not depend upon z and H depends only upon y. Property (i) implies that model (2) has invariant coordinate axes and that the equilibrium manifold of the fast and intermediate systems are the union of trivial and nontrivial manifolds. Property (ii) simplifies the analysis, as shown in the following.

3.1 Prey dynamics

The fast system (eq. (2a) with $y = const.$) has the trivial equilibrium manifold $x = 0$ and the nontrivial equilibrium manifold $F = 0$, which is

the parabola

$$y = \frac{r}{a_1}\left(1 - \frac{x}{K}\right)(b_1 + x)$$

in the (x, y) space. For $b_1 < K$ such a parabola is like in Fig.2: its maximum is

$$y_{\max} = \frac{r}{4Ka_1}(K + b_1)^2 \tag{3}$$

and its point of intersection with the y axis is

$$y_0 = \frac{rb_1}{a_1}$$

For $y = y_{\max}$ the fast system has a fold bifurcation, while for $y = y_0$ it has a transcritical bifurcation. The trivial manifold is stable above point y_0 because $f_x = F = \frac{a_1}{b_1}(y - y_0)$, while the nontrivial manifold is stable on the right branch of the parabola because $f_x = xF_x = xF_y y_x$ and F_y is positive. Thus, the fast segments of the singular orbits are oriented like in Fig.2.

3.2 Predator dynamics

The intermediate system (eq. (2b) with $z = const.$) is defined on the manifold $f = 0$, *i.e.*, on $x = 0$ and $F = 0$, and intermediate segments of singular orbits lie in a plane parallel to the (x, y) plane. It is therefore useful to represent the behavior of the intermediate system in such a plane, where the manifold $F = 0$ is the parabola shown in Fig.2.

Four cases of interest are presented in Fig.3 for increasing values of z. The manifold $G = 0$ varies with z, while the parabola $F = 0$ is independent upon z. Since $G > 0$ [$G < 0$] above [below] the manifold $G = 0$, the direction of the flow of the intermediate segments is immediately identified (see two arrow orbits on the parabola and on the y axis). The intermediate system has three or four equilibria: the origin and the points indicated by A, B and K. In the same figure two singular orbits of the (fast-intermediate) system, obtained by properly concatenating fast and intermediate segments, are also shown. They start from points 1 and 2 and tend toward an equilibrium point or toward the singular limit cycle (V y_{max} y_{min} R). More precisely, in Fig.3a (small value of z) both singular orbits tend toward the singular limit cycle. In Fig.3b the first singular orbit tends toward the limit cycle while the other tends toward the equilibrium K: there are therefore two singular attractors in this case. In Fig.3c both singular orbits tend toward point K which is a globally stable equilibrium for the (fast-intermediate) system. Finally, in Fig.3d (high value of z) there are two singular attractors,namely the equilibrium points A and K. For higher values of z, points A and B of Fig.3d disappear through a fold bifurcation and point K becomes a globally stable equilibrium point for the (fast-intermediate) system.

It must be noted that point $y_{\min}$ of the singular limit cycle in Fig.3 is below point y_0. This means that the intermediate segment of the singular

orbit starting from y_{max} lies partly on the unstable equilibrium manifold of the fast system. In other words, the singular orbit develops at intermediate speed along the stable trivial branch of the equilibrium manifold of the fast system, reaches the transcritical point y_0, and then develops further along the unstable branch of the same manifold. This somehow counterintuitive fact can be justified by noting that in an $\varepsilon-$neighborhood of point $(0, y_{\min})$ of Fig.3 both x and F are order ε so that $\dot{x}$ is order ε^2 while $\dot{y}$ is order ε, so that the orbit of system (2) develops almost vertically along the y axis. This holds until point y_{min} is reached where the increment of x accumulated below point y_0 compensates the decrement of x from y_{max} to y_0. The relationship between y_{min} and y_{max} is given by the following integral equation (see [15], [16], as well as [17], [18] for more general forms)

$$\int_{y_{\min}}^{y_{\max}} \frac{F(0,y)}{yG(0,y,z)} dy = 0 \tag{4}$$

Taking into account eqs. (2a), (2b) and (3) such a relationship can be given the form

$$\begin{aligned} &\tfrac{a_1}{b_1 d_1}\left(\tfrac{r(K+b_1)^2}{4Ka_1} - y_{\min}\right) - \tfrac{rb_2}{b_2 d_1 + a_2 z}\left(\ln \tfrac{r(K+b_1)^2}{4Ka_1} - \ln y_{\min}\right) + \\ &+ \left(\tfrac{rb_2}{b_2 d_1 + a_2 z} - \tfrac{r}{d_1} - \tfrac{a_1 a_2 z}{b_1 d_1^2}\right)\left[\ln\left(\tfrac{r(K+b_1)^2}{4Ka_1} + b_2 + \tfrac{a_2 z}{d_1}\right) - \ln\left(y_{\min} + b_2 + \tfrac{a_2 z}{d_1}\right)\right] = 0 \end{aligned} \tag{5}$$

Moreover, it can be proved [16] that the function $y_{\min}(z)$, implicitly defined by eq. (5), is decreasing with respect to z.

The results presented in this subsection are summarized in Fig.4, where the equilibria and limit cycles of the (fast-intermediate) system are shown in the three-dimensional space (x, y, z). The surface densely covered by limit cycles is called *cycle manifold* from now on. The four dots indicate the four bifurcation points of that system with respect to z. The four plots in Fig.3 are slices not passing through the four dots of this three-dimensional diagram.

3.3 Superpredator dynamics

The slow system (eq. (2c)) can now be used to determine the slow segments of the singular orbits. Since $\dot{z} > 0$ $[< 0]$ above [below] the manifold (plane)

$$y = \frac{b_2 d_2}{c_2 - d_2} \tag{6}$$

it is straightforward to conclude that the line $x = K,\ y = 0$ in Fig.4 is a slow segment of singular orbit developing from the right to the left, as well as the lowest part of the line $F = G = 0$. By contrast, the highest part of the same line develops from the left to the right.

3.4 Singular homoclinic orbit

The intersection of the plane $H = 0$ with the line $F = G = 0$ is an equilibrium point. If parameters are such that plane (6) is below point 2 in Fig.4, the equilibrium is a singular saddle S because one fast segment tends to it and

one intermediate segment (as well as the slow segment $F = G = 0$) comes from it. Fig.5 shows the singular orbit coming out from the singular saddle S. The first segment $S\ A$ is at intermediate speed and is followed by a segment $A\ B$ at slow speed and then by a new intermediate segment bringing the orbit on the cycle manifold. The coordinates z_A and z_B of points A and B are related one to each other by the following integral equation (similar to eq. (5))

$$\int_{z_A}^{z_B} \frac{G(K,0,z)}{zH(0)} dz = 0$$

which gives rise to

$$\left(\frac{a_1 K}{1+b_1 K} - d_1\right) \ln \frac{z_A}{z_B} = a_2 (z_A - z_B) \tag{7}$$

Once the singular orbit is on the cycle manifold, it stays on it and develops slowly to the right by covering it densely, because $\dot{z} > 0$ (recall that point 2 is above point S and that $y_{\min}(z)$ is decreasing with respect to z). When the singular orbit reaches point 2 it abandons the cycle manifold and goes to point Q with a segment at intermediate speed. Then, again, a slow motion develops from Q to R, where (see eq. (7))

$$\left(\frac{a_1 K}{1+b_1 K} - d_1\right) \ln \frac{z_Q}{z_R} = a_2 (z_Q - z_R) \tag{8}$$

From point R the singular orbit goes on the cycle manifold and develops on it for the second time until point 2 is reached. Thus, a singular cycle is

closed, as clearly indicated in Fig.5. From the same diagram it is also clear that a singular homoclinic orbit is obtained if parameters are such that the saddle S coincides with point 2. In such a case the outcoming segment of the saddle is 2 Q and the incoming segment is P 2.

4 Numerical results

From the above discussion, it follows that the singular homoclinic orbit is completely identified by four relationships, namely the three equations $F(x,y) = G(x,y,z) = H(y) = 0$ and eq. (5) with $y_{\min}$ substituted by y (this equation forces point S to coincide with point 2 in Fig.5). These four equations have in general one solution if one parameter is left free. Once a solution of these four equations has been obtained, eq. (8) with z_Q equal to the z coordinate of the saddle can be used to derive z_R. In this way the singular homoclinic orbit is fully identified geometrically.

Once a singular homoclinic orbit has been obtained, one can continue the solution of the four above mentioned equations and produce singular homoclinic bifurcation curves in any two dimensional parameter space. Fig.6 shows one of these singular bifurcation curves (dashed line) in the parameter space (K,r). Of course, the interest in such a singular bifurcation curve relies upon the conjecture that for nearby parameter values there exist homoclinic

orbits of system (2) with small values of ε. A proof of this conjecture has been given in [11] for the simple case of second order systems but is not yet available for third order systems (1) with generic functions f, g, and h. On the other hand, a proof constrained to the specific food chain model considered in this paper would be of very scarce interest. For this reason, only numerical results are presented here to prove that the conjecture holds for system (2).

Three homoclinic bifurcation curves of system (2) corresponding to three different values of ε are shown in Fig.6. They have been produced in two steps. First, an homoclinic orbit for a small value of ε has been obtained by simulation (see point A in Fig.6 and Fig.7a). Then, this orbit has been used as initial solution to produce a homoclinic bifurcation curve through continuation (this method is described in [4] and has been implemented in HOMCONT, an AUTO86 (see [19]) driver described in [20]). The two other bifurcation curves shown in Fig.6 has been produced in the same way. Only segments of the curves for $\varepsilon = 0.05$ and $\varepsilon = 0.1$ are shown in the figure because the complex geometry of the homoclinic orbit made the computations particulary hard.

Four homoclinic orbits are shown in Fig.7. The first (Fig.7a) corresponds to point A in Fig.6 ($\varepsilon = 0.05$, $K = 2.4778$, $r = 4.0$) and is very similar to the singular orbit shown in Fig.5. The second and the third (Figs.7b,c)

corresponds to points B and C of Fig.6, respectively, (B : $\varepsilon = 0.1$, $K = 2.09$, $r = 4.0$; C : $\varepsilon = 0.2$, $K = 1.8632$, $r = 4.0$), and are characterized by a smaller number of loops. These figures confirm that for $\varepsilon \to 0$ the homoclinic orbit tends toward the singular homoclinic orbit. Of course, for higher values of ε the homoclinic orbit might change its form and become an homoclinic orbit to a complex saddle like the one shown in Fig.7d that has been obtained by continuation starting from point C' in Fig.6.

5 Conclusion

The standard Rosenzweig-MacArthur model of tri-trophic food chains has been proved to have homoclinic orbits for suitable values of its parameters. The proof is based on a very simple and elegant geometric approach derived from singular perturbation analysis. The approach allows one to prove only the existence of singular homoclinic orbits and has therefore been integrated by extensive numerical analysis.

The approach can certainly be applied to many other third order nonlinear systems and is potentially of great value in population dynamics, where finding the consequences of the interactions between very fast and very slow components of complex ecosystems is a problem of major concern [21].

Acknowledgments

This paper was written at the International Institute for Applied Systems Analysis, Laxenburg, Austria, where the first author has participated into the 1996 IIASA Young Scientists Summer Program. The work has been financially supported by the Italian Ministry of Scientific Research and Technology, contract MURST 40% Teoria dei sistemi e del controllo. The authors are grateful to Yuri A. Kuznetsov, CWI, Amsterdam for his suggestions and advice.

References

[1] A. Klebanoff and A. Hastings. Chaos in three species food chains, *J. Math. Biol.* 32:427-451 (1994).

[2] K. McCann and P. Yodzis. Bifurcation structure of a three species food chain model, *Theor. Pop. Biol.* 48:93-125 (1995).

[3] Yu. A. Kuznetsov and S. Rinaldi. Remarks on food chain dynamics, *Math. Biosci.* 134:1-33 (1996).

[4] A. R. Champneys and Yu. A. Kuznetsov. Numerical detection and continuation of codimension-two homoclinic bifurcations, *Int. J. Bifurcation and Chaos* 4:785-822 (1994).

[5] R. E. O'Malley. *Introduction to Singular Perturbations*, Academic Press, New York, 1974.

[6] S. Muratori. An application of the separation principle for detecting slow-fast limit cycles in a three-dimensional system, *Appl. Math. Mod.* 43:1-18 (1991).

[7] S. Muratori and S. Rinaldi. Low- and high-frequency oscillations in three-dimensional food chain systems, *SIAM J. Appl. Math.* 52:1688-1706 (1992).

[8] S. Muratori and S. Rinaldi. Remarks on competitive coexistence, *SIAM J. Appl. Math.* 49:1462-1472 (1989).

[9] D. Ludwig, D. D. Jones and C. S. Holling. Qualitative analysis of insect outbreak systems: the spruce budworm and forest, *J. Anim. Ecol.* 47:315-332 (1978).

[10] S. Rinaldi and S. Muratori. Limit cycles in slow-fast forest-pest models, *Theor. Pop. Biol.* 41:26-43 (1992).

[11] Yu. A. Kuznetsov, S. Muratori and S. Rinaldi. Homoclinic bifurcations in slow-fast second order systems, *Nonlinear Analysis, Theory, Methods and Applications* 25:747-762 (1995).

[12] A. N. Tikhonov. Systems of differential equations containing small parameters at derivatives, *Mat. Sb.* 31:575-586 (1952). (In Russian.)

[13] L. C. Pontryagin. Asymptotic behavior of solutions of systems of differential equations with a small parameter at higher derivatives, *Izv. Akad. Nauk. SSSR Ser. Math.* 21:605-626 (1957). (In Russian.)

[14] V. I. Arnold, V. S. Afraimovich, Yu. S. Il'yashenko and L. P. Shil'nikov. Bifurcation theory, in *Dynamical Systems*, D. V. Anosov and V. I. Arnold, eds., VINITI, Moscow, 1986.

[15] M. Schecter. Persistent unstable equilibria and closed orbits of singularly perturbed equations, *J. Diff. Eqns.* 60:131-141 (1985).

[16] S. Rinaldi and S. Muratori. Slow-fast limit cycles in predator-prey models, *Ecol. Modelling.* 61:287-308 (1992).

[17] F. Diener and M. Diener. Seven formulas concerning canards, *C. R. Acad. Sci. Paris* 297:577-580 (1983). (In French.)

[18] A. K. Zvokin and M. A. Shubin. Non-standard analysis and singular perturbations of ordinary differential equations, *Russ. Math. Survs.* 39:69-131 (1984).

[19] E. Doedel and J. Kernévez. AUTO: Software for continuation problems in ordinary differential equations with applications. California Institute of Technology Technical report, Applied Mathematics, (1986).

[20] A. R. Champneys, Yu. A. Kuznetsov and B. Sandstede. HOMCONT: an AUTO86 driver for homoclinic bifurcation analysis. CWI Technical Report, AM-R9516, Amsterdam, (1995).

[21] C. S. Holling. The resilience of terrestrial ecosystems: local surprise and global change, in *Sustainable Development of the Biosphere*, W. C. Clark and R. E. Munn, eds., Cambridge University Press, Cambridge, UK, 1986.

Figure legends

Figure 1

A singular orbit of system (1). Single, double and triple arrows indicate slow, intermediate and fast segments of the singular orbit. The function f [h] is negative [positive] above the manifold $f = 0$ [$h = 0$], while g is positive on the right of the manifold $g = 0$.

Figure 2

Fast (three arrows) segments of singular orbits in the space (x, y). Heavy [dashed] lines indicate the stable [unstable] equilibrium manifold of the fast system.

Figure 3

Fast (three arrows) and intermediate (two arrows) segments of singular orbits of the fast-intermediate system (z increases from (a) to (d)).

Figure 4

Cycles and equilibria of the fast-intermediate system.

Figure 5

The singular saddle S and its singular outcoming orbit.

Figure 6

Singular homoclinic bifurcation curve (dashed line) and homoclinic bifurcation curves (continuous line) of system (2) for $\varepsilon = 0.05$, $\varepsilon = 0.1$, and $\varepsilon = 0.2$. Parameter values are $a_1 = 5/3$, $b_1 = 1/3$, $c_1 = 5/3$, $d_1 = 4/10$, $a_2 = 1/20$, $b_2 = 1/2$, $c_2 = 1/20$, $d_2 = 1/100$.

Figure 7

Four homoclinic orbits of system (2): (a), (b), (c) and (d) correspond respectively to points A, B, C and D in Fig.6. The orbit in (d) is a homoclinic orbit to a complex saddle obtained for $\varepsilon = 1.0$, the saddle has eigenvalues $\lambda_1 = -2.2144$, $\lambda_{2,3} = 0.0766 \pm i0.0331$.

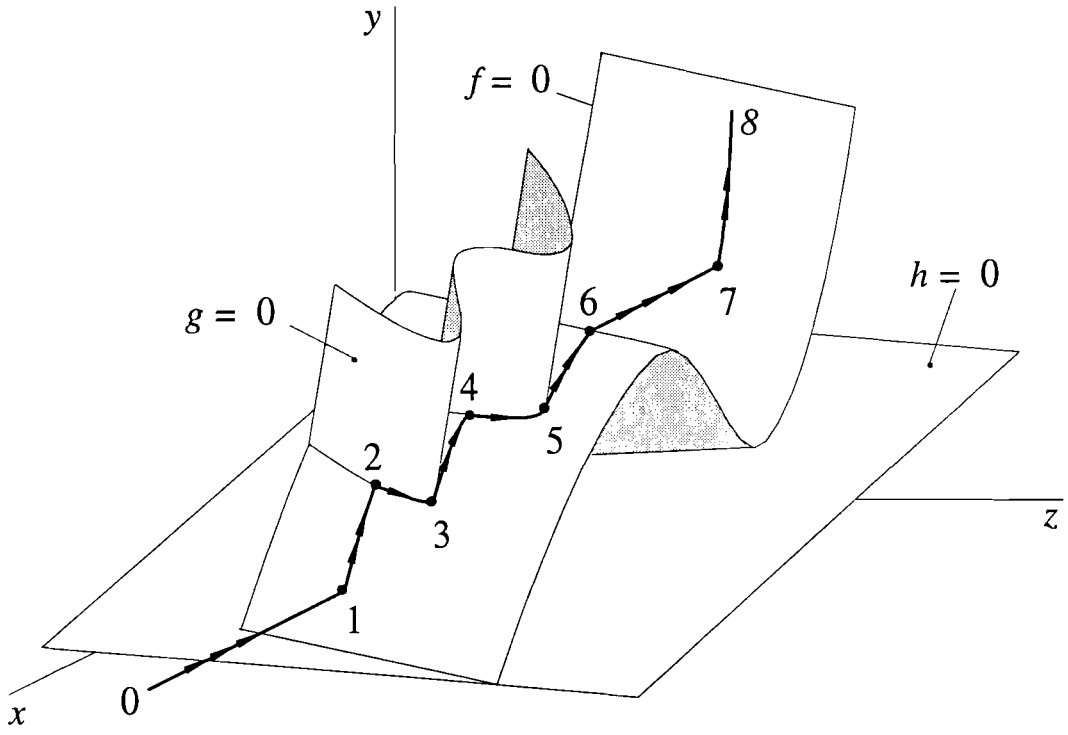

Figure 1

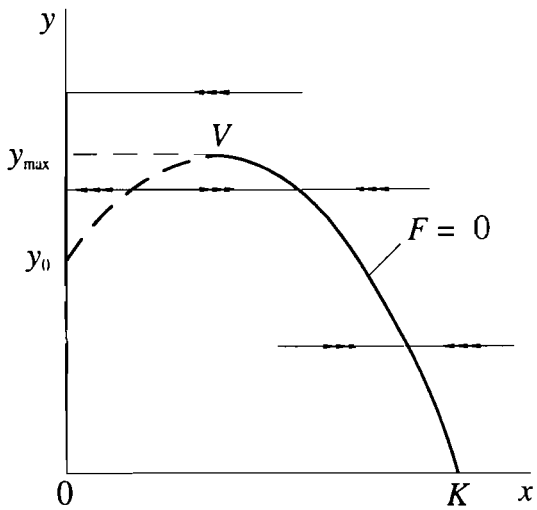

Figure 2

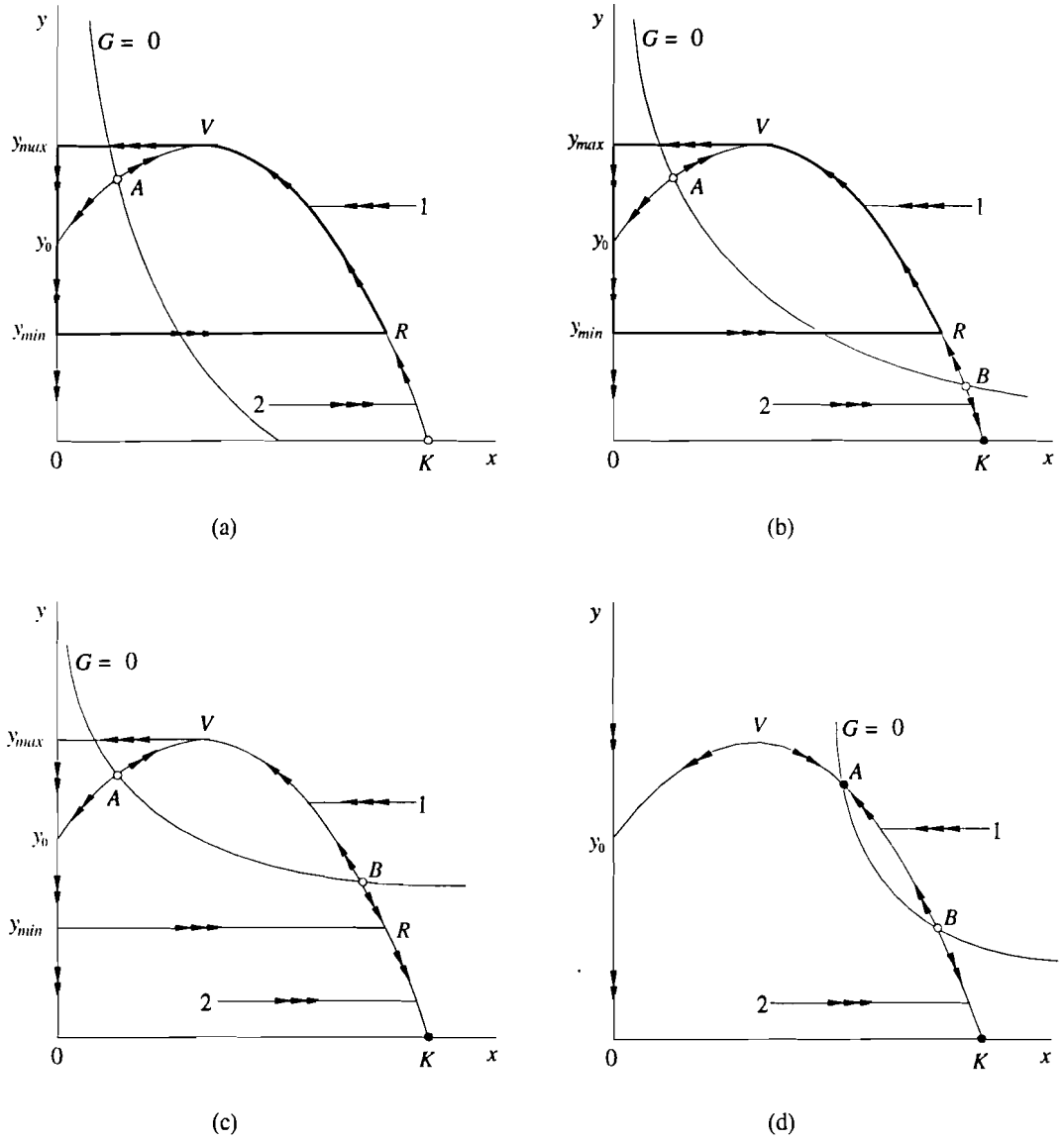

Figure 3

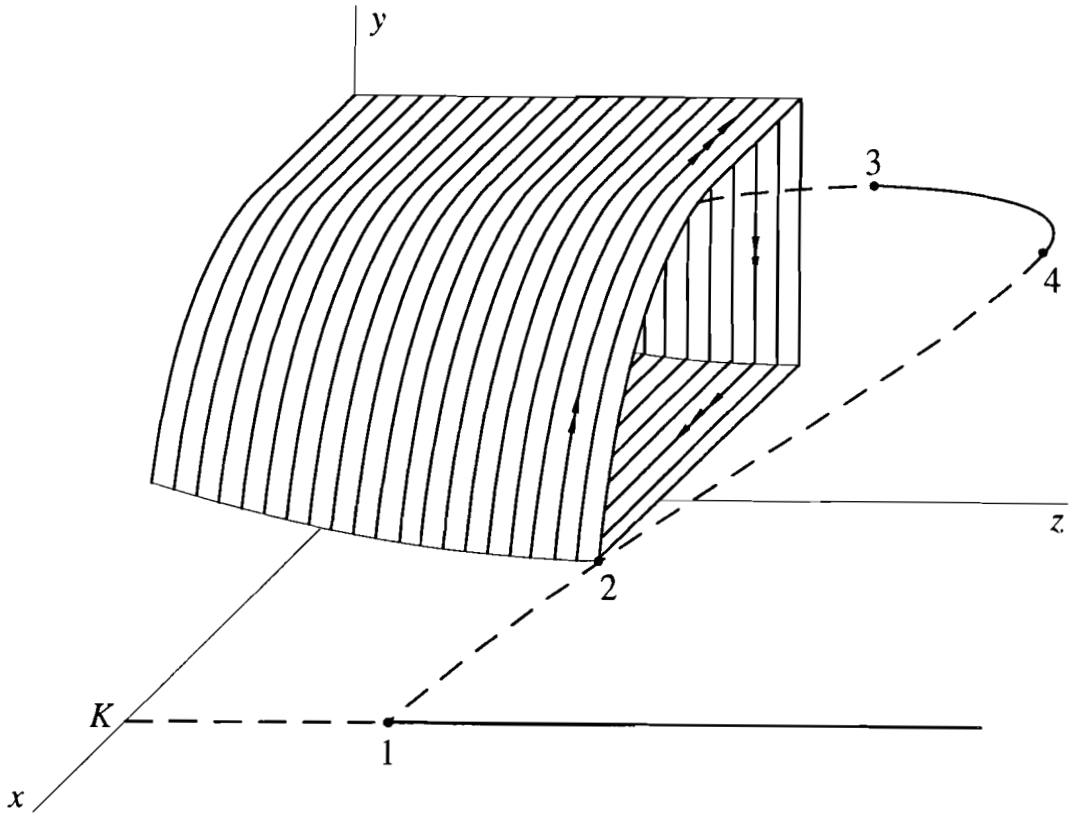

Figure 4

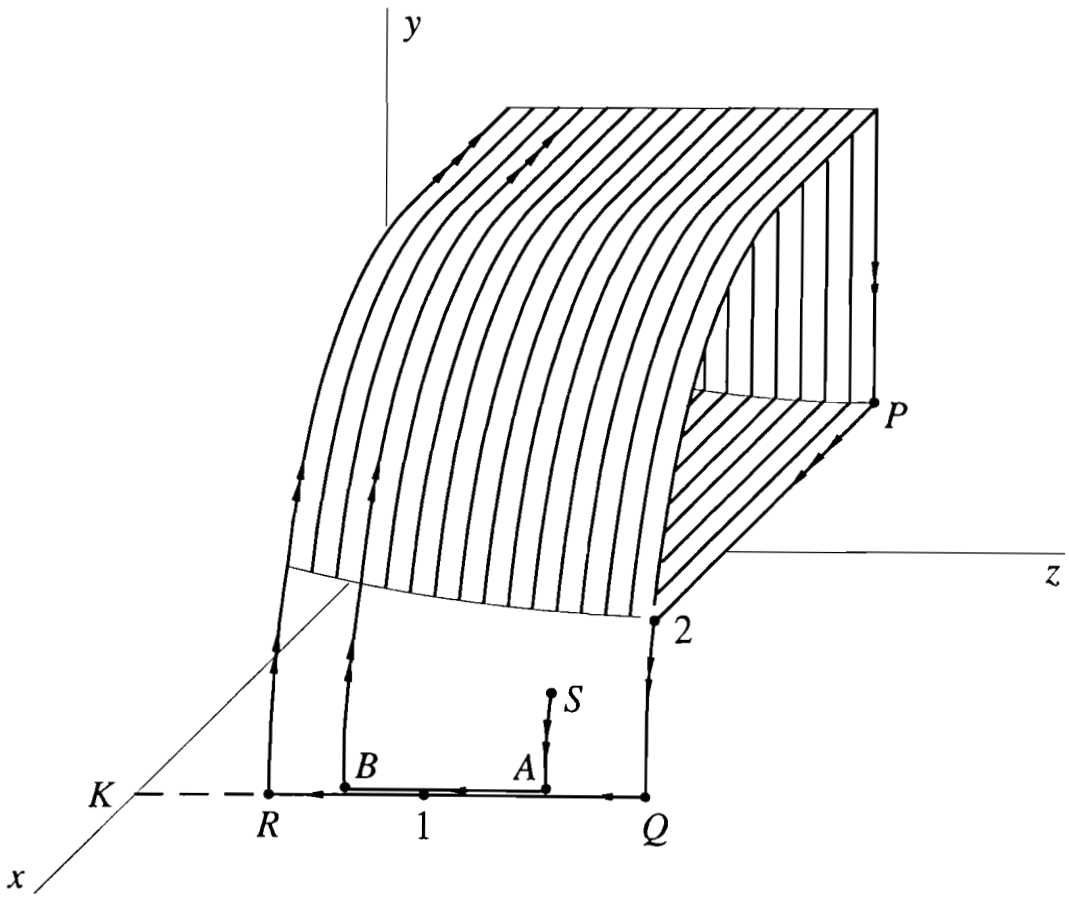

Figure 5

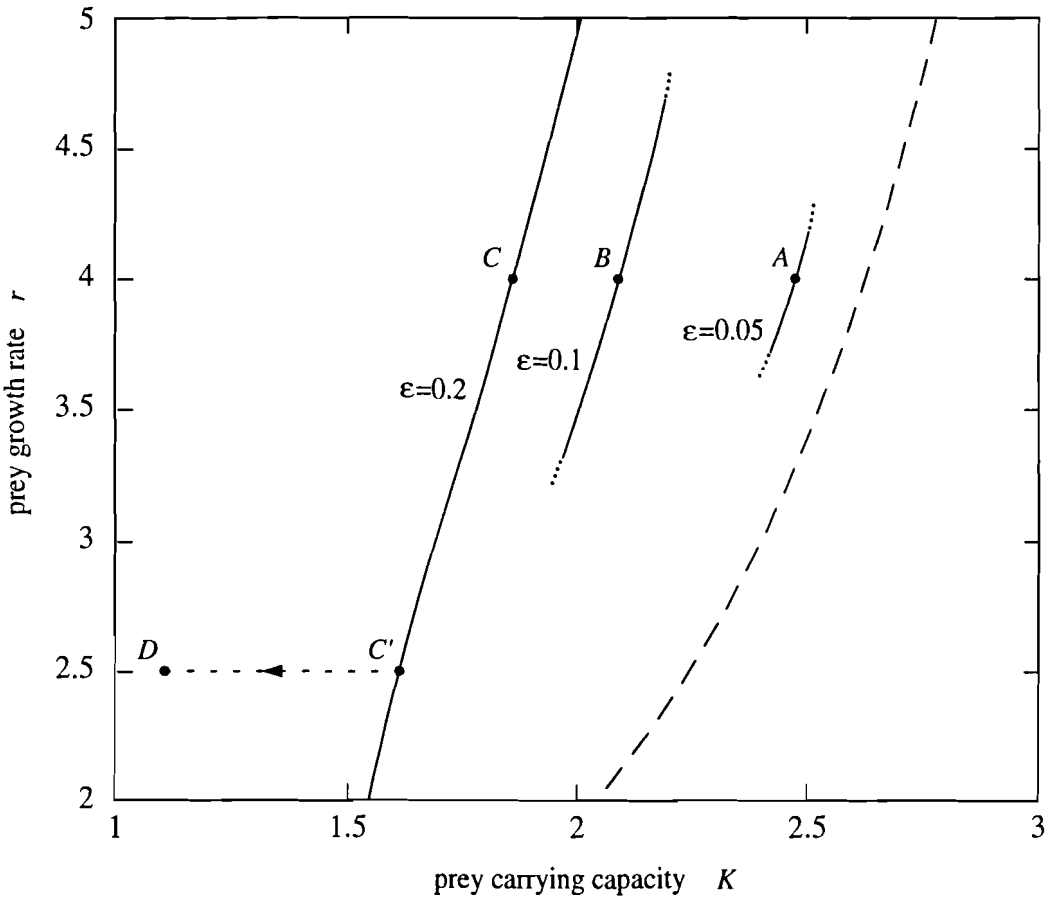
5
4.5
4
3.5
3
2.5
2
1
1.5
2
2.5
3
prey growth rate r
prey carrying capacity K
A
B
C
C'
D
ε=0.05
ε=0.1
ε=0.2

Figure 6

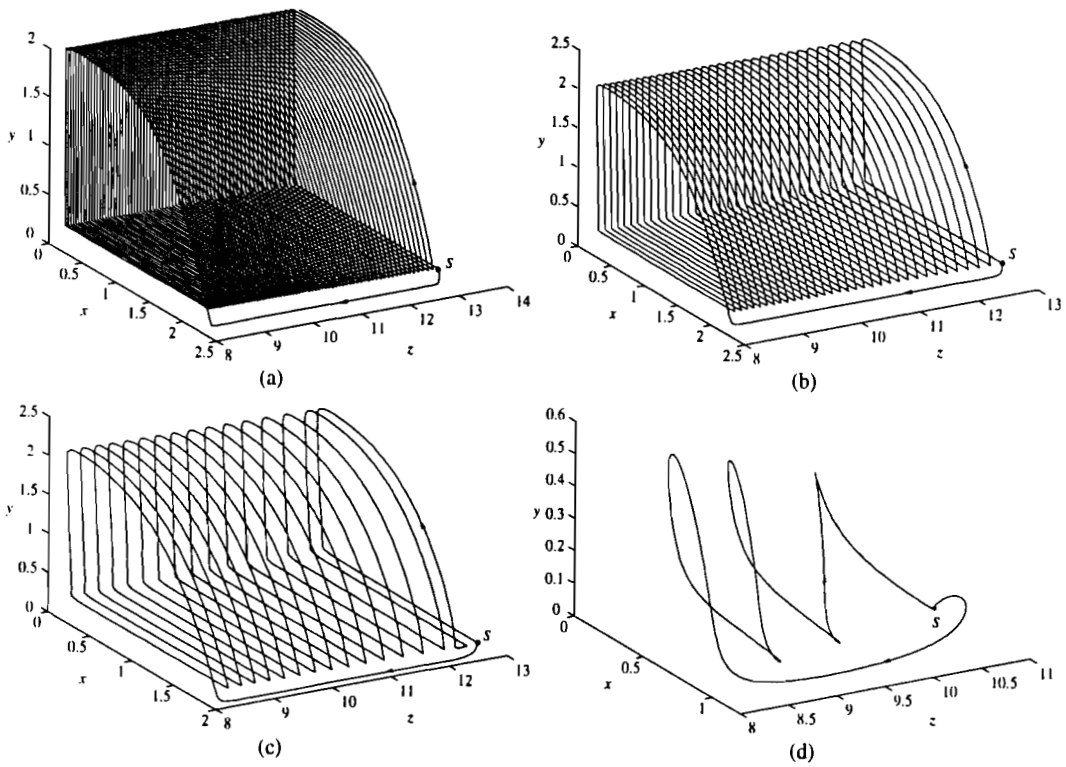

Figure 7